Effect of the Type of Carbon Nanotubes on Tribological Properties of Polyamide 6

Luis F. Giraldo,[1,2] Betty L. López,[1] Witold Brostow[2]
[1] *Grupo Ciencia de los Materiales, Instituto de Química, Universidad de Antioquia, Calle 62 #52-59 Torre 1 Lab 310, Medellín, Colombia*

[2] *Laboratory of Advanced Polymers & Optimized Materials (LAPOM), Department of Materials Science and Engineering, University of North Texas, Denton, Texas 76203-5310*

Multiwalled carbon nanotubes have been synthesized by catalytic chemical vapor deposition of ethylene, using two different catalysts in order to obtain nanotubes with average diameters of 24 and 58 nm, and different lengths. Polyamide 6 (PA6) was reinforced by melt-mixing in an extruder with 2 wt% functionalized and unfunctionalized carbon nanotubes (CNTs). The nanocomposites were characterized by thermogravimetric analysis, differential scanning calorimetry, and sliding wear determination (SWD). SWD results show a reduction of the residual depth in a scratch test. The reduction is larger in the presence of unfunctionalized CNTs. A further reduction is obtained when decreasing the nanotubes diameter, an effect which is related to larger interfaces between the nanotube and polymeric matrix. CNTs enhance the crystallinity of the polymer and act as nucleation sites, thus increasing the crystallization temperature in respect to neat PA6. The addition of carbon nanotubes helps the formation of PA6 in α-crystalline form, which is thermodynamically more stable that the γ-form. CNTs also can act as heterogeneous nucleation sites, hampering the movement of the polymer chains and increasing the crystallization temperature. POLYM. ENG. SCI., 49:896–902, 2009.

INTRODUCTION

Polymer tribology seems to be an underappreciated area; however, Rabinowicz has demonstrated the importance of tribology, including from the point of view of financial wellbeing of the industry [1]. Tribology deals with the interaction of surfaces in movement, including wear, friction, adhesion, and lubrication. Wear is the most expensive constituent of tribology [1]. Tribology initially developed for metals cannot be simply transferred to polymer-based materials (PBMs) because of a variety of manifestations of viscoelasticity by the latter [2]. Approaches in use to improve PBM tribology have been reviewed [3]. Primary challenges are the reduction of wear and friction in order to conserve and reduce the energy, lower costs, and increase the productivity. Fillers are known to provide a relatively easier usable option to improve properties of polymers [4–7]. More specifically, carbon nanotubes (CNTs) as a filler have been reported to provide mechanical strength along with flexibility [8–10].

Polyamide 6 (PA6) is one of the principal thermoplastics used in the textile industry and plastics engineering [11]. It is highly crystalline, exhibits good thermal stability and is often classified as a high performance polymer. Several materials have been used as fillers of PA6 such as clays [12–14], nanoparticles of nonporous silica [15], and also CNTs introduced by melt-mixing [16–19] or in situ [20]. Among these fillers, CNTs are promising; because of their high aspect ratio, they can be considered as one-dimensional (1D) nanomaterials. Moreover, CNTs can provide relatively homogeneous dispersion in polymeric matrices, improving the interfacial adhesion and the stress transference from the polymer to the filler. As discussed by Kopczynska and Ehrenstein [21], surface and interface interactions are decisive for the composite properties.

Previously, we have demonstrated that CNTs improve some tribological properties of PA6, specifically reducing the penetration depth in microscratch testing [22]. In this work, different carbon nanotubes are synthesized and used to reinforce PA6. The effect of the diameter and length of the carbon nanotubes as well as their modification on thermal and tribological properties of PA6 is thus determined.

Correspondence to: Luis F. Giraldo; e-mail: luis.giraldo@gmail.com
Contract grant sponsor: The Robert A. Welch Foundation, Houston; contract grant number: B-1203; contract grant sponsor: Universidad de Antioquia, Medellin and COLCIENCIAS, Bogota (Apoyo a la comunidad cientifica nacional a traves de doctorados nacionales).
DOI 10.1002/pen.21386
Published online in Wiley InterScience (www.interscience.wiley.com).

EXPERIMENTAL

Synthesis of Carbon Nanotubes

The carbon nanotubes were synthesized using catalytic chemical vapor deposition (CCVD) of ethylene using different types of catalysts as described elsewhere in more detail [15]. Generally, 1.0 g of catalyst of 6 wt% Fe (impregnated in mesoporous silica MCM41 (Fe/MCM41) or a bimetallic catalyst 6 wt% Fe + 12% wt% Co supported on $CaCO_3$ (Fe-Co/$CaCO_3$) was placed in a quartz tube with 25 mm of diameter and heated up to 750°C under nitrogen atmosphere; then 300 cm^3/min of ethylene mixed with 100 cm^3/min of nitrogen were flowing through the quartz tube for 30 min. The oven was subsequently cooled down to room temperature under nitrogen atmosphere.

The nanotubes synthesized on mesoporous support were purified using 20% hydrofluoric acid (Merck); those synthesized on $CaCO_3$ (Merck) were purified with18% aq. nitric acid (Merck). The samples were filtrated, washed with deionized water, and dried overnight at 100°C.

Multiwalled CNTs (MWCNTs) synthesized on Fe-Co/$CaCO_3$ were functionalized with 68% aq. nitric acid in a reflux apparatus for 24 h. After, the MWCNTs were washed with plenty of deionized water and dried at 80°C overnight.

FTIR

Functionalized MWCNTs were dispersed in a KBr pill and analyzed by Fourier transformed infrared spectrophotometry (FTIR, Perkin-Elmer, Spectrum One) in the transmittance mode.

Reinforcement of PA6

Neat polymer was reinforced with 2 wt% MWCNTs by melt-mixing using a corotative twin-screw extruder (type Rheomex PTW-16/25p from Thermo Haake) with four heating zones from 230 to 250°C at 100 rpm.

Sample Preparation

Samples for scratch test were prepared by compression molding at 250°C at 17.2 MPa. Two Teflon films and two polished stainless steel platens were used. The pellets were placed in a 4 cm × 4 cm mold with the thickness of 2 mm and covered with Teflon films and plates. When the plates were in contact with the heated compression molding platen after reaching the desired temperature, they were held at that temperature for 5 min. The pressure of 6.9 MPa was applied for 2 min, and then the final pressure was increased to 17.2 MPa. In the last step, molded specimens were cooled to room temperature.

Scratch Testing

Tests are carried out on a CSM Micro-Scratch Tester (MST), from Neuchatel, Switzerland, as in earlier work [23–28]. Sliding wear determination (SWD) is performed by multiple scratching along the same groove (15 times) [3, 24, 28] performed under the following conditions: normal load 15.0 N; scratch length 5.0 mm; 5 mm/minute indenter speed at room temperature (24°C). A conical diamond indenter was used in all the tests with the diameter of 200 μm and the cone angle 120°. The instantaneous penetration depth R_p and the residual (healing) depth R_h are thus determined as a function of the number of runs.

Microscopy Analysis

JEOL JSM T-300 scanning electron microscope (SEM) was used. The nanocomposites were sputter coated with a thin layer of gold for 3 min so as to achieve conductivity in the samples. CNTs were placed in 5 ml of absolute ethanol and sonicated for 20 min, and a drop of the suspension was placed on the sample support.

Thermal Analysis

The thermogravimetric analysis (TGA) was performed in a Q500 machine from TA Instruments. The nanocomposites and carbon nanotubes were heated up to 800°C at 10 K/min in air. Differential scanning calorimetry (DSC) results were obtained on a Q100 machine from TA Instruments. The nanocomposites were heated up to 250°C and left at this temperature for 5 min, subsequently were cooled down to room temperature and heated again at 10 K/min up to 250°C. Finally, nonisothermal crystallization was achieved by cooling at 20 K/min until room temperature.

RESULTS AND DISCUSSIONS

Carbon Nanotubes Characterization

Figure 1 shows SEM images of nanotubes synthesized on Fe-Co/$CaCO_3$ and Fe/MCM41 with corresponding diameter distributions. As it can be seen, the nanotubes synthesized on calcium carbonate as support present a broader diameter distribution than those synthesized on mesoporous silica. Apparently in the latter case, a large silica surface area helps to disperse iron clusters, providing locations to carbon nanotubes with lower diameters, good structural regularity, and higher length values. However, while the carbon yield using Fe/MCM41 catalyst is around 45% from TGA analysis, for the Fe-Co/$CaCO_3$ catalyst the yield is considerably higher and around 60%. As it is indicated by the arrows in the Fig. 1, in both samples some particles of amorphous carbon still remain after acidic purification.

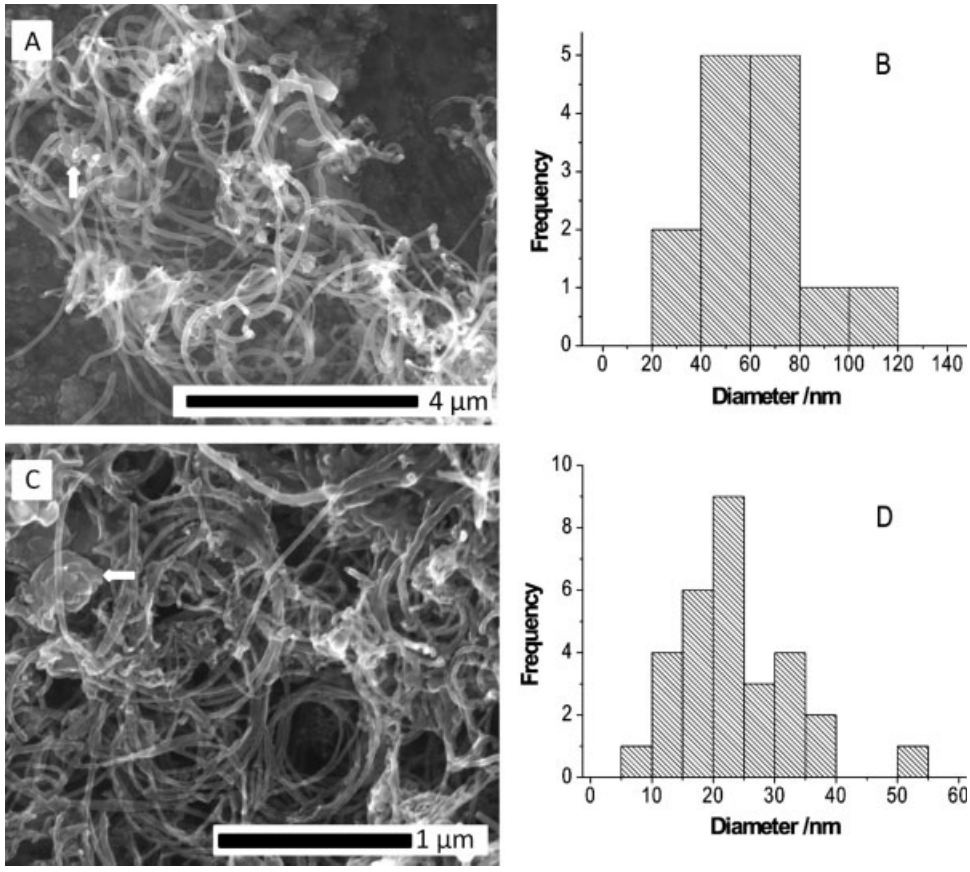

FIG. 1. SEM micrographs of MWCNTs synthesized using Fe-Co/($CaCO_3$) (A,B) and Fe/MCM41 (C,D) with the corresponding diameter distributions.

Figure 2 (left) shows TGA results for purified carbon nanotubes. MWCNTs synthesized on mesoporous support show a weight loss of 98%, whereas those synthesized on calcium carbonate have the loss of 90%. In the latter case, 10% of residual particles are inside the carbon nanotubes and they can catalyze early decomposition of CNTs reducing their thermal stability.

Figure 2 (right) displays the FTIR spectra of the functionalized CNTs. Bands at 2923 cm^{-1} and 2859 cm^{-1} are assigned to the stretching of saturated C—H bonds, whereas the peak at 1729 cm^{-1} corresponds to the stretching of carbonyl groups. New chemicals bonds are principally formed at the ends or in the structural defects of nanotubos, such as ring of five-seven carbon atoms,

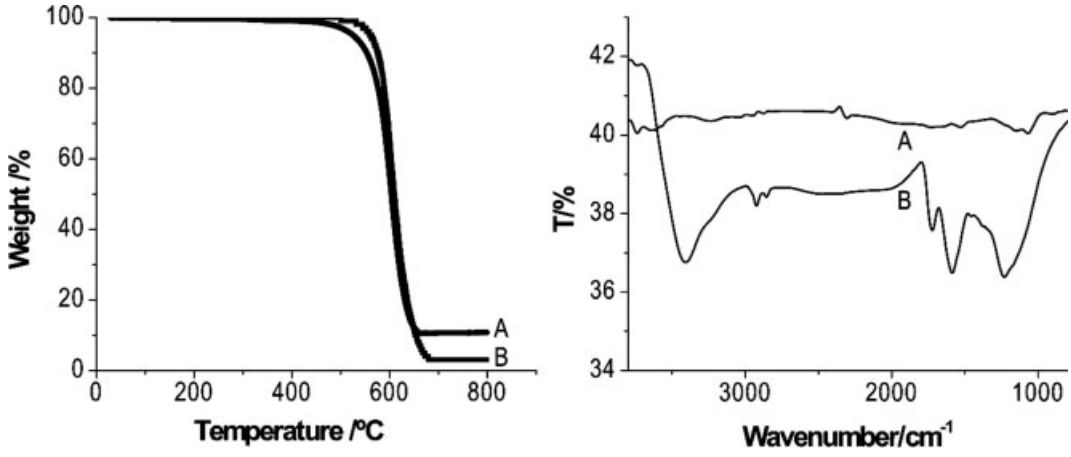

FIG. 2. Left: TGA of MWCNTs synthesized on Fe-Co/$CaCO_3$ (A) and Fe/MCM41 (B). Right: FTIR of MWCNTs (Fe-Co/$CaCO_3$) unfunctionalized (A) and functionalized (B).

 DOI 10.1002/pen

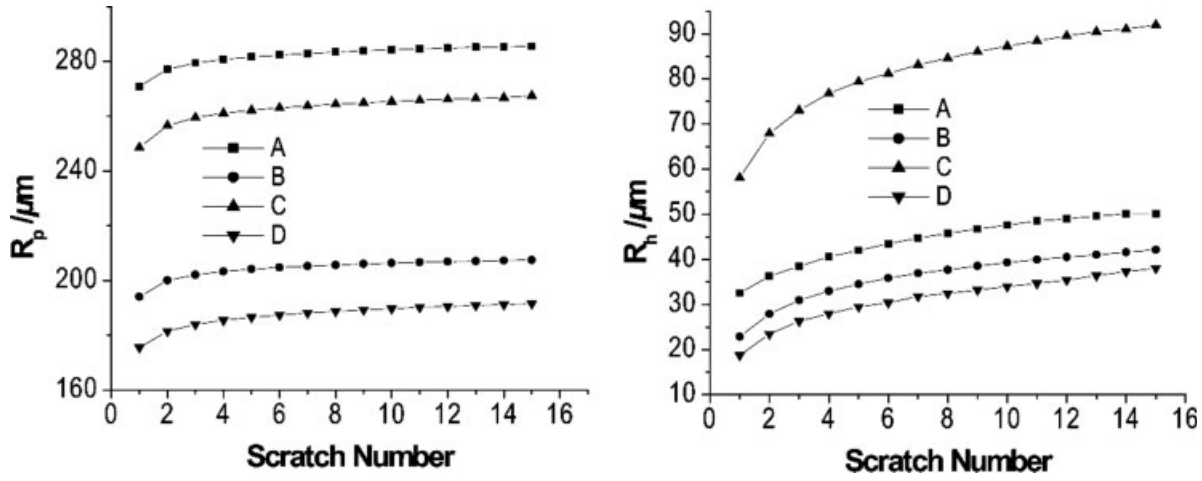

FIG. 3. R_p and R_h results as a function of the number of runs along the same groove; PA6 (A), PA6 + 2 wt% MWCNTs ($CaCO_3$) (B), PA6 + 2 wt% functionalized MWCNTs ($CaCO_3$) (C) and PA6 + 2 wt% MWCNTs (MCM41) (D).

which present higher reactivity in relation to six member ring. The presence of OH groups is confirmed for the band at 3408 cm^{-1}. Carbon nanotubes are highly flexible and they are often in contact; therefore, it is possible that several hydroxyl and carboxylic groups get in contact, making possible hydrogen bonds between the tubes.

Sliding Wear Results

Figure 3 shows instantaneous penetration depth R_p and residual penetration depth R_h values determined as described earlier. Multiple scratching leads to an asymptote in the diagram of R_p as function of the scratch number; strain hardening behavior discovered previously [24] is also seen here. As previously discussed [28, 29], most polymers show this kind of behavior; polystyrene (PS) is an exception, a fact which led to a quantitative definition of brittleness [28] and a demonstration how brittle PS is [29].

As can be seen in Fig. 3, early indentations produce larger effects. With respect to pure PA6, the R_p values are considerably reduced by addition of MWCNTs. The reduction is larger for nanotubes with a lower diameter synthesized using the Fe/MCM41 catalyst.

Functionalized CNTs reduce only slightly the penetration depth of PA6 as compared to unfunctionalized nanotubes. A possible explanation: interfacial adhesion between the filler and polymer can be enhanced by the functionalization, but the melt-mixing process suppresses the free movement of the nanotubes due to its high viscosity and it can impede adequate dispersion of the nanotubes in the polymeric matrix [30]. It is possible also that this restricted movement of nanotubes due to the van der Waals forces and hydrogen bonds between the functionalized nanotubes make the tubes agglomerate which would reduce the stress transfer from the polymer to the filler. There are other regions in the polymer in which the carbon nanotubes can be well dispersed and are interacting with the polymeric chains possibly by means of the amide groups in the PA6 and hydroxyl groups in the tube, which reduces the chains movement and impedes the recovery of the polymer. This can be supported by the highest R_h values in the right part of Fig. 3 for functionalized CNTs.

Figure 3 right shows also that the final position of indenter is lower for the PA6 reinforced with thinner nanotubes, apparently due to the greater exposed contact areas between the nanotubes and polymer. For the same applied load, but using 1 wt% MWCNTs produced by arc discharge (highly agglomerated), we had obtained deeper R_h values for nanocomposites than for neat PA6 [22], similar

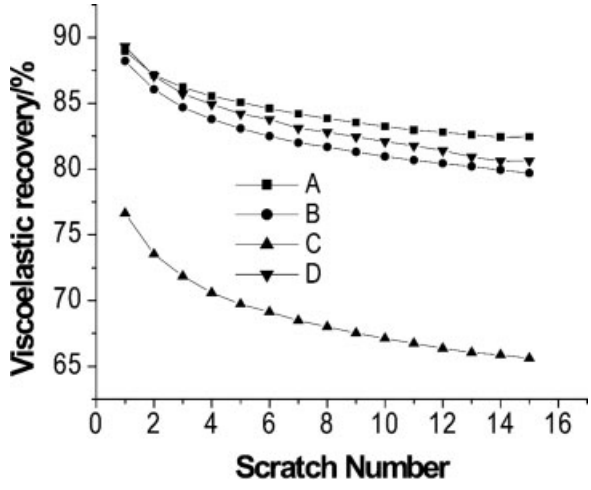

FIG. 4. Viscoelastic recovery (healing) in sliding wear determination of PA6 (A), PA6 + 2 wt% MWCNTs ($CaCO_3$) (B), PA6 + 2 wt% functionalized MWCNTs ($CaCO_3$) (C) and PA6 + 2 wt% MWCNTs (MCM41) (D).

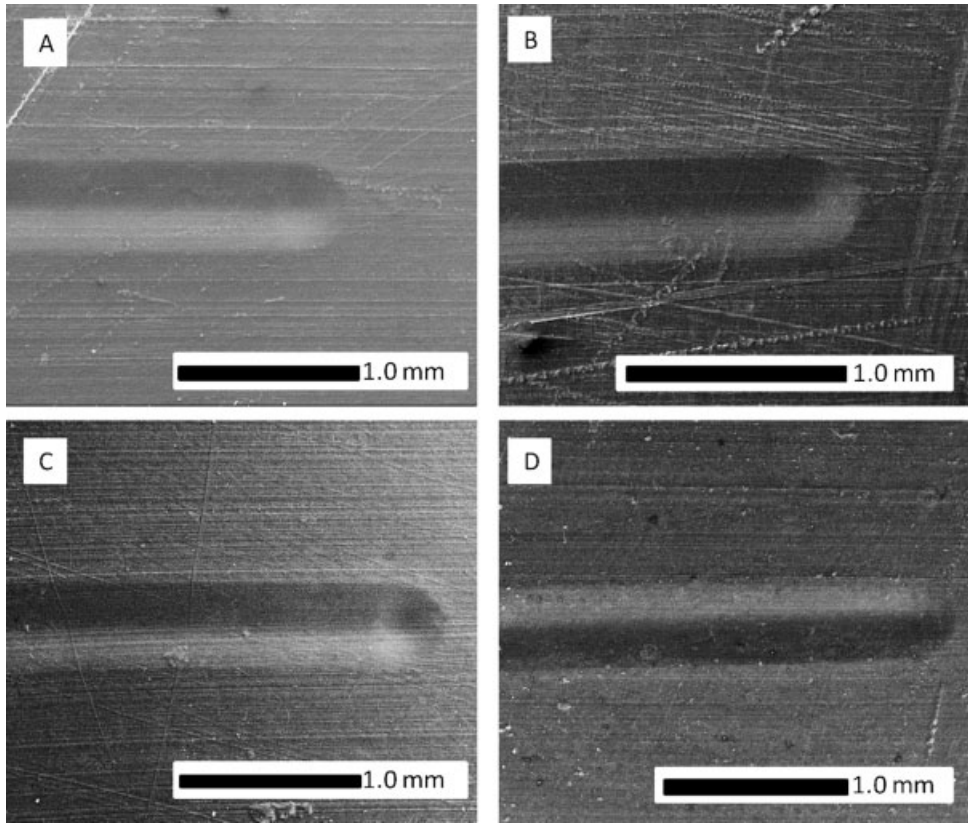

FIG. 5. Scratch grooves for PA6 (A), PA6 + 2 wt% MWCNTs ($CaCO_3$) (B), PA6 + 2 wt% functionalized MWCNTs ($CaCO_3$) (C) and PA6 + 2 wt% MWCNTs (MCM41) (D) as seen in SEM.

to the behavior of functionalized nanotubes seen in Fig. 3 right and already commented upon. However, Fig. 3 also shows us that the filler nanotubes with smaller diameter provide the highest reduction in R_h in SWD.

Viscoelastic recovery (healing) ϕ in scratch or sliding wear testing has been defined [3, 23] as

$$\phi = (1 - R_h/R_p) \times 100\% \quad (1)$$

Figure 4 shows results obtained from *Eq. 1*. The presence of nanotubes hampers the viscoelastic recovery, confirming earlier results [22]. The results for the nanocomposites are only slightly worse than those for neat PA6; an exception again are the results for composites containing functionalized CNTs-for reasons already discussed earlier.

Scratching grooves seen in SEM are shown in Fig. 5. All the grooves present one channel or a single line without debris on the polymer surface-behavior characteristic for PA6 [26, 27]. It is possible to see a broader groove for the polymer without reinforcement (see also Table 1); in this respect, CNTs provide better scratch and wear resistance. Stuart and Briscoe reported that deeper grooves are also wider [31]. This agrees with our results—except for the functionalized nanotubes, a result which can also be explained by the tubes agglomeration.

Under certain assumptions [31–33], groove width can be also related to the so-called scratch hardness H_s:

$$H_s = 4P/\pi d^2 \quad (2)$$

Here P is the load applied, and d is the scratch width.

The results of using *Eq. 2* are presented in Table 1. The neat PA6 with the widest groove has the lowest hardness.

Thermophysical Characteristics

DSC results are presented in Fig. 6. The polymer melting point does not change significantly.

There is a slight increase in the crystallinity upon the addition of CNTs, due to the increase in the melting enthalpy by the CNTs as summarized in Table 2. The

TABLE 1. Scratch hardness.

Sample	*P*/*N*	*d* (μm)	$H_s \cdot 10^6$ (N μm^{-2})
PA6	15	512	72.8
PA6 + 2% MWCNTs ($CaCO_3$)	15	470	86.5
PA6 + 2% MWCNTs ($CaCO_3$) f	15	478	83.6
PA6 + 2% MWCNTs (MCM41)	15	465	88.3

 DOI 10.1002/pen

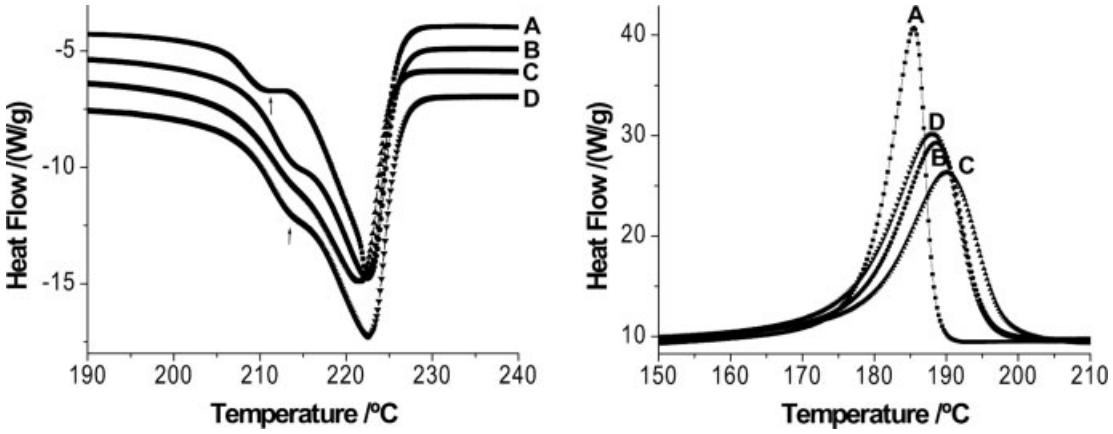

FIG. 6. Thermograms of PA6 nanocomposites; melting (left) and nonisothermal crystallization (right). PA6 (A), PA6 + 2 wt% MWCNTs ($CaCO_3$) (B), PA6 + 2 wt% functionalized MWCNTs ($CaCO_3$) (C) and PA6 + 2 wt% MWCNTs (MCM41) (D).

increase could be related to better crystal perfection as is suggested by a smaller size and displacement to higher temperatures of the small shoulder associated with the less stable γ crystal of PA6 at 210°C; the more thermodynamically stable α-form has the melting temperature $T_m = 222$°C [6, 32, 33].

Figure 6 (right) shows that the crystallization temperature of the polymer increases with the addition of 2 wt% CNTs from 185°C for neat PA6 to 190°C (lower diameter CNTs). The nanotubes might serve as the nucleation sites for the polymer crystals to grow and a reduction of the chain mobility has been demonstrated by dynamic mechanical analysis [21].

Table 2 summarizes thermophysical properties. The percentage of crystallity X_c was calculated as the relation between the enthalpy of fusion ΔH_m for a given composition and ΔH_m^o (240 J/g), where the latter corresponds to the average between the crystalline phases γ and α.

Figure 7 shows the thermogravimetric analyses for the nanocomposites. The thermal stability is slightly improved with the incorporation of CNTs with an average diameter <58 nm synthesized on $CaCO_3$, showing once again the importance of the contact surface between the nanotubes and the matrix. The functionalized nanotubes show the same thermal behavior as those without functionalization and for brevity are not included in the diagram. Also once again thinner nanotubes provide better interactions with PA6, limiting the diffusion of oxygen molecules through the matrix, thus delaying the polymer decomposition as seen in onset decomposition temperature.

TABLE 2. T_m, T_c, ΔH_c, ΔH_m, and X_c for the nanocomposites of PA6[a].

Sample	T_m (°C)	T_c (°C)	ΔH_m (J/g)	ΔH_c (J/g)	X_c (%)
PA6	222.4	185.5	56.5	64.0	23.5
PA6 + 2% MWCNTs ($CaCO_3$)	222.5	188.5	66.3	65.1	28.1
PA6 + 2% MWCNTs ($CaCO_3$) f[b]	222.5	188.9	57.6	56.7	24.5
PA6 + 2% MWCNTs (MCM41)	221.6	190.0	67.2	69.4	28.6

[a] Above T_c, temperature of crystallization; T_m, melting temperature; ΔH_m, enthalpy of fusion; ΔH_c, enthalpy change of crystallization; X_c, crystallinity.

[b] f, functionalized.

CONCLUSIONS

The carbon nanotubes reduce the instantaneous penetration depth R_p in the PA6 after the multiple scratch tests. When the CNTs diameter is smaller, bigger stress transference from the polymer to the filler can be obtained in the nanocomposite due to the higher surface of contact between the polymer and nanotubes and a bigger reduction in R_p is achieved.

The acidic functionalization of CNTs did not considerably increase the scratch resistance possibly for the inadequate dispersion of the reinforcement agent because of

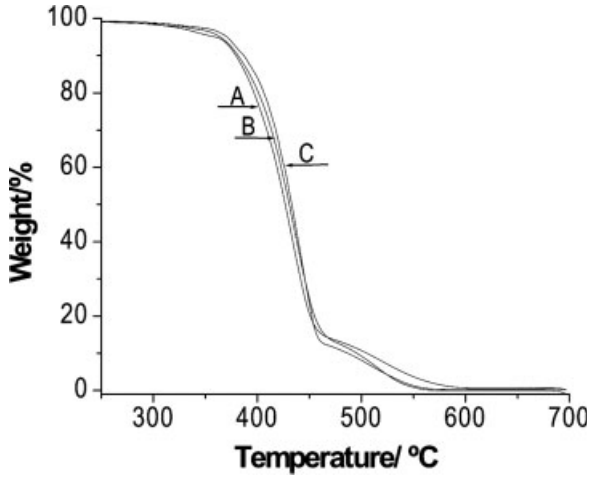

FIG. 7. TGA of PA6 (A), PA6 + 2 wt% MWCNTs ($CaCO_3$) (B), PA6 + 2 wt% MWCNTs (MCM41) (C).

the strong interaction among nanotubes, which could promote its agglomeration and reduce the dispersion degree of CNTs in the polymer.

The carbon nanotubes constitute an alternative promissory in order to develop textile materials with high performance due to the increase in the tribological properties as use wear of these polymeric matrices.

REFERENCES

1. E. Rabinowicz, *Friction and Wear of Materials*, 2nd ed., Wiley, New York (1995).
2. W. Brostow, Ed., *Performance of Plastics*, Hanser, Munich, Cincinnati (2000).
3. W. Brostow, J.-L. Deborde, M. Jaklewicz, and P. Olszynski, *J. Mater. Ed.*, **25**, 119 (2003).
4. V. Kovacevic, S. Lucic, D. Hace, and A. Glasnovic, *Polym. Eng. Sci.*, **36**, 1134 (1995).
5. J.E. Mark, *Polym. Eng. Sci.*, **36**, 2905 (1995).
6. V. Kovacevic, D. Packham, S. Lucic, D. Hace, and I. Smit, *Polym. Eng. Sci.*, **39**, 1433 (1999).
7. M. Rabello, *Aditivaçao de Polimeros*, Artliber, São Paulo (2000).
8. A. Huczko, *Appl. Phys. A.*, **74**, 617 (2002).
9. V.N. Popov, *Mater. Sci. Eng. Rep.*, **43**, 61 (2004).
10. J.W. Mintmire and C.T. White, *Carbon*, **33**, 893 (1995).
11. E.B. Mano, *Polimeros como Materiais de Engenharia*, Edgard Blücher, São Paulo (1996).
12. D.M. Lincoln, R.A. Vaia, Z.G. Wang, and B.S. Hsiao, *Polymer*, **42**, 1621 (2001).
13. T.D. Fornes and D.R. Paul, *Polymer*, **44**, 3945 (2003).
14. C. Ibanes, M. de Boissieu, L. David, and R. Seguela, *Polymer*, **47**, 5071 (2006).
15. L.F. Giraldo, M. Echeverri, and B.L. López, *Macromol. Symp.*, **258**, 119 (2007).
16. B. Schartel, P. Potschke, U. Knoll, and M. Abdel-Goad, *Eur. Polym. J.*, **41**, 1061 (2005).
17. P.V. Kodgire, A.R. Bhattacharyya, S. Bose, N. Gupta, A.R. Kulkarni, and A. Misra, *Chem. Phys. Lett.*, **432**, 480 (2006).
18. O. Meincke, D. Kaempfer, H. Weickmann, C. Friedrich, M. Vathauer, and H. Warth, *Polymer*, **45**, 739 (2004).
19. A.R. Bhattacharyya and D. Fischer, *Macromol. Chem. Phys.*, **206**, 2084 (2005).
20. J. Gao, M.E. Itkis, A. Yu, E. Bekyarova, B. Zhao, and R.C. Haddon, *J. Am. Chem. Soc.*, **127**, 3847 (2005).
21. A. Kopczynska and G.W. Ehrenstein, *J. Mater. Ed.* **29**, 325 (2007).
22. L.F. Giraldo, W. Brostow, E. Devaux, B.L. López, and L.D. Pérez, *J. Nanosci. Nanotech.*, **8**, 3176 (2008).
23. W. Brostow, B. Bujard, P.E. Cassidy, H.E. Hagg, and P. Montemartini, *Mater. Res. Innovat.*, **6**, 7 (2002).
24. W. Brostow, G. Darmarla, J. Howe, and D. Pietkiewicz, *e-Polymer*, **025**, 1 (2004).
25. M.D. Bermudez, W. Brostow, F.J. Carrion-Vilches, J.J. Cervantes, and D. Pietkiewicz, *e-Polymer*, **001**, 1 (2005).
26. M.D. Bermudez, W. Brostow, F.J. Carrion-Vilches, J.J. Cervantes, G. Damarla, and J.M. Perez, *e-Polymer*, **003**, 1 (2005).
27. M.D. Bermudez, W. Brostow, F.J. Carrion-Vilches, J.J. Cervantes, and D. Pietkiewicz, *Polymer*, **46**, 347 (2005).
28. W. Brostow, H.E. Hagg Lobland, and M. Narkis, *J. Mater. Res.* **21**, 2422 (2006).
29. W. Brostow and H.E. Hagg Lobland, *Polym. Eng. Sci.* **48**, 1982 (2008).
30. R. Haggenmueller, H.H. Gommans, A.G. Rinzlerb, J.E. Fischer, and K.I. Winey, *Chem. Phys. Lett.* **330**, 219 (2000).
31. B. Stuart and B. Briscoe, *Polym. Int.*, **38**, 95 (1995).
32. I.Y. Phang, J. Ma, L. Shen, T. Liu, and W.-D. Zhang, *Polym. Int.*, **55**, 71 (2006).
33. L. Sun, J.-T. Yang, G.-Y. Lin, and M.-Q. Zhong, *Mater. Lett.*, **61**, 3963 (2007).

 DOI 10.1002/pen